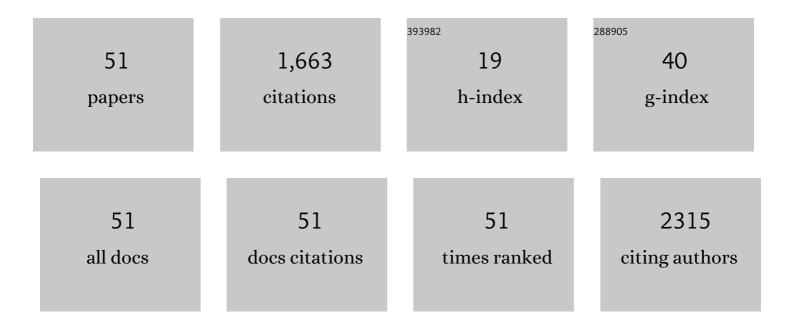
## Xiaodong Hao

List of Publications by Year in descending order

Source: https://exaly.com/author-pdf/8361658/publications.pdf Version: 2024-02-01



#	Article	IF	CITATIONS
1	Three-dimensional porous MXene/layered double hydroxide composite for high performance supercapacitors. Journal of Power Sources, 2016, 327, 221-228.	4.0	253
2	Nickel-Manganese Layered Double Hydroxide Nanosheets Supported on Nickel Foam for High-performance Supercapacitor Electrode Materials. Electrochimica Acta, 2016, 194, 179-186.	2.6	208
3	Amorphous/Crystalline Heterostructured Cobaltâ€Vanadiumâ€Iron (Oxy)hydroxides for Highly Efficient Oxygen Evolution Reaction. Advanced Energy Materials, 2020, 10, 2002215.	10.2	198
4	Atomicâ€Scale Valence State Distribution inside Ultrafine CeO <sub>2</sub> Nanocubes and Its Size Dependence. Small, 2018, 14, e1802915.	5.2	77
5	pH-Dependent Degradation of Methylene Blue via Rational-Designed MnO <sub>2</sub> Nanosheet-Decorated Diatomites. Industrial & Engineering Chemistry Research, 2014, 53, 6966-6977.	1.8	65
6	Preparation, characterization and dye adsorption of Au nanoparticles/ZnAl layered double oxides nanocomposites. Applied Surface Science, 2013, 283, 505-512.	3.1	64
7	Layer-by-layer self-assembled two-dimensional MXene/layered double hydroxide composites as cathode for alkaline hybrid batteries. Journal of Power Sources, 2018, 390, 208-214.	4.0	56
8	Rational design of hierarchically porous birnessite-type manganese dioxides nanosheets on different one-dimensional titania-based nanowires for high performance supercapacitors. Journal of Power Sources, 2014, 270, 675-683.	4.0	54
9	Engineering birnessite-type MnO2 nanosheets on fiberglass for pH-dependent degradation of methylene blue. Journal of Physics and Chemistry of Solids, 2015, 83, 40-46.	1.9	50
10	Facile synthesis of CoAl-LDH/MnO2 hierarchical nanocomposites for high-performance supercapacitors. Ceramics International, 2014, 40, 2115-2120.	2.3	49
11	One-pot controllable synthesis of flower-like CoFe2O4/FeOOH nanocomposites for high-performance supercapacitors. Materials Letters, 2014, 123, 229-234.	1.3	47
12	Fe-doping induced localized amorphization in ultrathin α-Ni(OH) <sub>2</sub> nanomesh for superior oxygen evolution reaction catalysis. Journal of Materials Chemistry A, 2021, 9, 14372-14380.	5.2	44
13	Ni/Mn and Al Dual Concentration-Gradients To Mitigate Voltage Decay and Capacity Fading of Li-Rich Layered Cathodes. ACS Energy Letters, 2021, 6, 2755-2764.	8.8	42
14	Controlled deposition of Au on (BiO) <sub>2</sub> CO <sub>3</sub> microspheres: the size and content of Au nanoparticles matter. Dalton Transactions, 2015, 44, 8805-8811.	1.6	34
15	MnO <sub>x</sub> -modified ZnAl-LDOs as high-performance adsorbent for the removal of methyl orange. Dalton Transactions, 2014, 43, 6667-6676.	1.6	32
16	Organic molecule confinement reaction for preparation of the Sn nanoparticles@graphene anode materials in Lithium-ion battery. Journal of Colloid and Interface Science, 2021, 589, 308-317.	5.0	25
17	Cluster Nanozymes with Optimized Reactivity and Utilization of Active Sites for Effective Peroxidase (and Oxidase) Mimicking. Small, 2022, 18, e2104844.	5.2	25
18	Direct Imaging for Single Molecular Chain of Surfactant on CeO <sub>2</sub> Nanocrystals. Small, 2018. 14. e1801093.	5.2	23

XIAODONG HAO

#	Article	IF	CITATIONS
19	Engineering one-dimensional and two-dimensional birnessite manganese dioxides on nickel foam-supported cobalt–aluminum layered double hydroxides for advanced binder-free supercapacitors. RSC Advances, 2014, 4, 63901-63908.	1.7	21
20	Facile biphasic synthesis of TiO2–MnO2 nanocomposites for photocatalysis. Ceramics International, 2016, 42, 19425-19428.	2.3	19
21	One-step synthesis of CeFeO <sub>3</sub> nanoparticles on porous nanocarbon frameworks derived from ZIF-8 for a boosted oxygen reduction reaction in pH universal electrolytes. Journal of Materials Chemistry A, 2022, 10, 13013-13020.	5.2	19
22	Self-assembled spongy-like MnO2 electrode materials for supercapacitors. Physica E: Low-Dimensional Systems and Nanostructures, 2012, 45, 103-108.	1.3	18
23	Atomistic origin of high-concentration Ce3+ in {100}-faceted Cr-substituted CeO2 nanocrystals. Acta Materialia, 2021, 203, 116473.	3.8	18
24	Defect-engineered ultrathin NiMoO4 nanomeshes as efficient and stable electrocatalysts for overall water splitting. Ceramics International, 2021, 47, 19098-19105.	2.3	18
25	A Novel Approach to Enhance Bone Regeneration by Controlling the Polarity of GaN/AlGaN Heterostructures. Advanced Functional Materials, 2021, 31, 2007487.	7.8	17
26	Modifying energy storage performances of new lead-free system ferroelectric capacitors through interfacial stress. Applied Surface Science, 2021, 559, 149992.	3.1	15
27	Controllable preparation of crystalline red phosphorus and its photocatalytic properties. Nanoscale, 2021, 13, 18955-18960.	2.8	15
28	Formation dynamics of mesocrystals composed of organically modified CeO <sub>2</sub> nanoparticles: analogy to a particle formation model. CrystEngComm, 2019, 21, 3836-3843.	1.3	14
29	Mn-doping tuned electron configuration and oxygen vacancies in NiO nanoparticles for stable electrocatalytic oxygen evolution reaction. Applied Surface Science, 2022, 577, 151952.	3.1	14
30	Rational design of manganese dioxide decorated skeleton of colloidal mesoporous carbon nanocomposites for supercapacitors. Ceramics International, 2014, 40, 13381-13388.	2.3	12
31	MXene-supported NiMn-LDHs as efficient electrocatalysts towards enhanced oxygen evolution reactions. Materials Advances, 2022, 3, 4359-4368.	2.6	12
32	Surfactant-mediated morphology evolution and self-assembly of cerium oxide nanocrystals for catalytic and supercapacitor applications. Nanoscale, 2021, 13, 10393-10401.	2.8	11
33	Increasing oxygen vacancies in CeO <sub>2</sub> nanocrystals by Ni doping and reduced graphene oxide decoration towards electrocatalytic hydrogen evolution. CrystEngComm, 2022, 24, 3369-3379.	1.3	9
34	Millimeter-scale laminar graphene matrix by organic molecule confinement reaction. Carbon, 2020, 161, 277-286.	5.4	8
35	Rational Design and Synthesis of Adjustable Pt and Pt-Based 3D-Nanoframeworks. ACS Applied Energy Materials, 2022, 5, 942-950.	2.5	8
36	SnCo Nanoalloy/Graphene Anode Constructed by Microfluidic-Assisted Nanoprecipitation for Potassium-Ion Batteries. ACS Applied Nano Materials, 2022, 5, 2616-2625.	2.4	8

XIAODONG HAO

#	Article	IF	CITATIONS
37	2D black arsenic phosphorus and its application for anodes of lithium ion batteries. CrystEngComm, 2020, 22, 8228-8235.	1.3	7
38	ONE-STEP AND CONTROLLABLE SELF-ASSEMBLY OF <font>Au/TiO<sub>2</sub></font> /CARBON SPHERES TERNARY NANOCOMPOSITES WITH A NANOPARTICLE MONOSHELL WALL. Nano, 2012, 07, 1250025.	0.5	6
39	Templated self-assembly of Au–TiO2 binary nanoparticles–nanotubes. Chinese Chemical Letters, 2014, 25, 874-878.	4.8	6
40	Effect of <i>in situ</i> degradation on the atomic structure and optical properties of GaN-based green light-emitting diodes. Applied Physics Letters, 2020, 117, .	1.5	6
41	Suspended hybrid films assembled from thiol-capped gold nanoparticles. Nanoscale Research Letters, 2012, 7, 295.	3.1	5
42	Low temperature photoluminescence study of GaAs defect states*. Chinese Physics B, 2020, 29, 010703.	0.7	5
43	The Surface Morphology Evolution of GaN Nucleation Layer during Annealing and Its Influence on the Crystal Quality of GaN Films. Coatings, 2021, 11, 188.	1.2	5
44	Electrochemical Performance of Graphene Oxide/Black Arsenic Phosphorus/Carbon Nanotubes as Anode Material for LIBs. Materials, 2022, 15, 4576.	1.3	5
45	The formation of island-shaped morphology on the surface of InGaN/GaN QWs and the enhancement of carrier localization effect caused by high-density V-shaped pits. Materials Science in Semiconductor Processing, 2021, 131, 105848.	1.9	4
46	Crystallization kinetics of amorphous red phosphorus to black phosphorus by chemical vapor transport. CrystEngComm, 2022, 24, 504-511.	1.3	4
47	Ultrafast synthesis of Au(I)-dodecanethiolate nanotubes for advanced Hg2+ sensor electrodes. Nanoscale Research Letters, 2014, 9, 601.	3.1	3
48	Improving the internal quantum efficiency of QD/QW hybrid structures by increasing the GaN barrier thickness. RSC Advances, 2020, 10, 41443-41452.	1.7	2
49	Effect of V-Shaped pits on optical properties of GaN-Based green light-emitting diodes. Optical Materials, 2020, 107, 110129.	1.7	2
50	Interfacial polygonal patterning via surfactant-mediated self-assembly of gold nanoparticles. Nanoscale Research Letters, 2013, 8, 436.	3.1	1
51	Cerium Valence State Distribution: Atomic-Scale Valence State Distribution inside Ultrafine CeO2 Nanocubes and Its Size Dependence (Small 42/2018). Small, 2018, 14, 1870195.	5.2	0